ELECTROPORATION BY STRONG INTERNAL DEFIBRILLATION SHOCK IN INTACT STRUCTURALLY NORMAL AND CHRONICALLY INFARCTED RABBIT HEARTS

By

SEOK CHAN KIM

Submitted in partial fulfillment of the requirements

For the degree of Master of Science

Thesis Adviser: Yuanna Cheng, M.D., Ph.D.

Department of Biomedical Engineering

CASE WESTERN RESERVE UNIVERSITY

January, 2008

CASE WESTERN RESERVE UNIVERSITY

SCHOOL OF GRADUATE STUDIES

We hereby approve the thesis of

SEOK CHAN KIM

candidate for the Master of Science degree *.

(Signed)

Xin Yu, Sc.D.
(Chair of the Committee)

Yuanna Cheng, M.D., Ph.D.

Dominique M. Durand, Ph.D.

(Date)

November 20, 2007

*We also certify that written approval has been obtained for any proprietary material contained therein.

TABLE OF CONTENTS

LIST OF FIGURES

Electroporation by Strong Internal Defibrillation Shock

in Intact Structurally Normal and Chronically Infarcted Rabbit Hearts

Abstract

by

Seok Chan Kim

A strong internal defibrillation shock may damage the heart via disruption of cell membranes (electroporation). The spatial distribution and extent of electroporation were characterized in intact rabbit hearts with and without chronic (>4 weeks) left ventricular myocardial infarction (MI). An implantable defibrillator was inserted in the right ventricle, and one monophasic shock (+300-V, 8-ms) was delivered by a 150-μF capacitor clinical defibrillator. Electroporation was assessed by uptake of membrane-impermeant propidium iodide into ventricular myocardium through electropores. In control (n=2) and MI (n=2) groups without shock, PI uptake was minimal. In both control (n=5) and MI (n=5) groups with shock, electroporation mostly occurred near the shock electrode, distributed along the active region of the shock electrode. In the MI group with shock, shock-induced electroporation was significantly increased ($p<0.05$) in the surviving epicardial layer of the infarcted region. Between the control and MI groups, the overall extent of electroporation was similar.

1. INTRODUCTION

Application of a defibrillation shock to the heart is the most effective and immediate therapy against lethal ventricular fibrillation. While the defibrillation shock can rescue patients from life-threatening arrhythmias, the shock may have unfavorable ramifications due to its excitatory and suppressive effects.[1-5] A strong electrical shock may also temporarily or permanently damage the heart via formation of aqueous pores referred to as electropores due to disruption of the cell membrane (electroporation).

Experimentally, electroporation is commonly used to provide access for transport of DNA, RNA, or other macromolecules into the intracellular space, and has been extensively studied.[6-9] The effects of electroporation on cardiac electrical activity have been investigated in isolated myocyte[10-12] and cardiac tissue[13-15] preparations. During measurements of the transmembrane potential change, elevated diastolic potential,[13, 16, 17] upwardly shifted or depolarized resting membrane potential, decreased action potential amplitude, and reduced rate of rise during the upstroke of action potential[3, 18] have been attributed to the occurrence of electroporation. Electroporation has also been incorporated into computer models of postshock transmembrane potential change in order to provide a better fit between empirical data and simulations, as well as to explain its role in defibrillation.[19-22]

Electroporation affects the cellular responses to an electrical shock and therefore, may play a crucial role in determining the overall response of the heart to a defibrillation shock. Although studies have been performed to evaluate the impact of electroporation on cardiac electrical activities as well as the effect of shock-induced transmembrane polarization pattern on defibrillation via the virtual electrode polarization hypothesis,[23-25]

the role of electroporation in defibrillation remains ambiguous.[3, 17, 21, 22, 26] More fundamentally, a question regarding the spatial distribution and extent of electroporation by a defibrillation shock in the intact heart has not been addressed.

Clinically, patients with a prior history of left ventricular (LV) myocardial infarction (MI) have an increased risk of lethal arrhythmia.[27-29] An implantable cardioverter defibrillator (ICD) lead is commonly implanted in the right ventricle (RV) of these patients to deliver rescue shocks that can terminate otherwise lethal arrhythmias. The infarct border zone (BZ) is an area characterized by reduced conduction velocity, gap junction reorientation, and decreased tissue anisotropy[30-34] following electrophysiological and structural remodeling of the surviving myocytes. As a result of this remodeling, the infarct BZ provides a substrate for shock-initiated reentry and an anchor that can stabilize reentrant arrhythmias.[4, 35, 36] Increased heterogeneity of myocardial structure in the infarct BZ may also accentuate shock-induced transmembrane polarization due to large values of activating function in areas of heterogeneity.[37-43] Consequently, the extent of electroporation may be more pronounced in the infarct BZ, and this may impact defibrillation failure or success. The spatial vulnerability of the MI heart to shock-induced electroporation, however, has never been studied.

To test the hypothesis that MI hearts may be more susceptible to electroporation due to internally delivered shock, the spatial distribution and extent of shock-induced electroporation were first characterized in intact, structurally normal rabbit hearts and rabbit hearts with healed myocardial infarction (more than 4 weeks post-MI). The vulnerability of MI hearts to shock-induced electroporation was then assessed by comparing the extent of electroporation between control and MI hearts. A membrane-

impermeant dye, propidium iodide (PI) was used to characterize electroporation.[6, 18, 44, 45] The spatial characterization of electroporation may be further used to advance targeted transportation of genes or drugs into the intracellular space[6, 46] and ablation therapy by electroporation.[47] Evaluation of the spatial distribution and extent of shock-induced electroporation may contribute to an improved understanding of the mechanisms of defibrillation, with respect to the occurrence and impact of electroporation. Spatial comparison of electroporation between the normal and MI hearts may aid identification of the pro- and anti-arrhythmogenic aspects of electroporation, and facilitate development of safer and more effective defibrillation therapies.

2. METHODS

2.1 Animal Model

The animal research protocol was approved by the Institutional Animal Care and Use Committee of the Cleveland Clinic. Animals included in this study were housed in the animal facility under veterinary supervision and received humane care as set forth in *Guide for the Care and Use of Laboratory Animals* published by the National Institutes of Health (NIH Publication No. 85-23, revised 1996).

14 adult New Zealand White rabbits of either sex weighing 3 to 4 kg (Harlan, Indianapolis, IN) were used in this study. 7 rabbits were used as controls in which no surgical infarction procedure was performed. A chronic MI was created in 7 rabbits, as described in detail previously.[4, 48] Briefly, the rabbits were anesthetized and intubated for the left thoracotomy. A long-lasting antibiotic was administered preoperatively. The heart rate, ECG, and oxygen and carbon dioxide saturation levels were continuously monitored. Depending on the branching pattern,[49, 50] the lateral or posterolateral division of the left coronary artery was identified. To minimize occurrence of ventricular arrhythmias, 1 mg/kg lidocaine was intravenously injected immediately before the ligature placement. The target artery was ligated approximately at a level of 40% from the apex. A chest tube was inserted, and the chest was closed by approximating the ribs on both sides of the incision. The chest was sealed by four suture layers, and the chest tube was withdrawn while negative pressure was applied. Postoperatively, an analgesic was given immediately following the surgery and twice a day thereafter for additional two days. Following infarction, the rabbits were allowed to heal at least for 4 weeks.

2.2 Heart Preparation

The acute heart preparation and experimental setup have also been described in detail.[4, 51, 52] Briefly, the intact control or MI heart was isolated and placed on the cannula of a modified Langendorff apparatus for *in vitro* retrograde perfusion via the aorta. Temperature- and pH-controlled, modified oxygenated Tyrode solution was filtered through 2-μm Millipore filters before perfusion through the heart. A custom-modified 10-mm coil (1.8 mm in diameter) defibrillation electrode was inserted into the RV cavity through the pulmonary artery. The distal tip was consistently positioned against the anterior RV free wall and the septum at the very apex (Figure 1). The shock electrode was composed of a 6-mm nonconducting inactive region and a 10-mm active region. The 50-mm coil reference electrode was placed in a U-shape with the arms pointing upward while completely immersed in the perfusion bath. The reference electrode was parallel to the posterior epicardial surface of the heart, positioned approximately 10 to 20 mm behind and above the tip of the apex. The reference electrode (RE) position is schematically illustrated in Figure 6A and Figure 7A. A bipolar pacing electrode was placed at the apex of the posterior RV to pace the heart at a basic cycle length of 300 ms.

2.3 Experimental Protocol

The heart was suspended and equilibrated in the Tyrode solution-filled perfusion chamber for 30 to 40 minutes (Figure 2). Fifteen minutes prior to shock delivery, the perfusate was changed to a Tyrode solution containing 30-μM PI (Sigma-Aldrich). In 5 control and 5 MI hearts, one +300-V, 8-ms truncated exponential monophasic shock was delivered by a 150-μF capacitor defibrillator (HVS-02; Ventritex, Sunnyvale, CA) during

the repolarization phase, approximately 100 ms following the QRS complex. A shock of high intensity (300 V) was used to ensure the occurrence of electroporation in this model. The anodal polarity was chosen because it is less likely to induce postshock arrhythmia compared to the cathodal monophasic shock. No postshock arrhythmia was induced in this study. Mean delivered energy and impedance recorded by the defibrillator were 5.8 ± 0.1 joules and 43 ± 2 ohms in the control group (n = 5) and 5.7 ± 0.0 joules (p = 0.14 versus control) and 46 ± 1 ohms ($p < 0.05$) in the MI group (n = 5). No shock was delivered in 2 control and 2 MI hearts. Postshock perfusion with 30-μM PI-containing Tyrode solution was continued for 15 minutes. During the 40-minute washout, the heart was perfused with Tyrode solution without PI. The heart was removed from the perfusion chamber and placed in ice-cold Tyrode solution to reduce cardiac contraction. The atria were excised, exposing the intact ventricles and the septum. The heart was embedded in cooled Tissue-Tek Embedding Medium (OCT; Sakura Finetek, Torrance, CA), frozen in cold isopentane (2-methybutane; Sigma-Aldrich, MO), and stored at -80˚C. 20-μm thick transverse sections were cut at -20˚C in 800-μm intervals from the apex toward the base, mounted onto Superfrost Plus micro slides (75x25 mm; VWR, West Chester, PA) or custom-ordered Superfrost Plus large slides (75x38 mm; Fisher Scientific, Houston, TX), and stored at -20˚C.

2.4 Fluorescence Study

The apex-to-base lengths of the ventricles from which samples were collected were 18.48 ± 1.73 mm in the control group (n = 7) and 18.70 ± 2.00 mm in the MI group (n = 7, p = 0.83). 12 ± 3 slides were visually selected from the full range of transverse

sections according to the PI fluorescence distribution pattern. PI fluorescence was imaged using a digital camera (RTE/CCD-1300 Y/HS; Roper Scientific, Trenton, NJ) on an epifluorescence microscope (DMRXA; Leica, Heidelberg, Germany) with a Texas Red filter (5X objective). The camera exposure (277 ± 60 ms) was kept constant within the same heart to minimize variations due to imaging condition. A motorized stage (H138 ProScan; Prior Scientific, Rockland, MA) and MetaMorph 6.21r1 software (Molecular Devices, Sunnyvale, CA) generated a mosaic image of the entire cross-section with 4 μm/pixel resolution. A representative transverse section from the control heart stained with PI upon shock delivery is shown in Figure 3. The entire ventricular myocardium was visualized and analyzed based on its inherent autofluorescence at exposure times in which localized PI-stained nuclei appeared brightly. Since segmented PI fluorescence only represented areas of nuclear staining (Figure 3A), electroporation was quantified as the total autofluorescent tissue area within the boundaries of PI accumulation. Representative tissue traced for positive PI staining is shown in Figure 3B. PI cluster boundary tracing and tissue area quantification were performed in an automated fashion using Image-Pro 6.2 (Media Cybernetics, Silver Springs, MD). The extent of electroporation was defined as PI-accumulated tissue volume normalized to the total tissue volume (%PI Volume). The total tissue volume was obtained via linear piecewise integration of myocardial cross-sectional areas along the long axis. PI-accumulated tissue volume was similarly integrated and quantified within the PI-cluster boundaries.

In analyzing the spatial extent of electroporation transversely with respect to the shock electrode position, the ventricles at each cutting plane was first divided into 4 regions (Figure 3B). The first region encompassed the anterior and anterolateral RV free

wall and approximately one-fourth of the septum (aRV) that was in a close vicinity to the shock electrode (SE). The three remaining regions were similarly categorized to include the posterior and posterolateral RV free wall and the adjacent septum (pRV), the anterior and anterolateral LV free wall and the adjacent septum (aLV), and the posterior and posterolateral LV free wall and the adjacent septum (pLV). In each of 4 regions except the aRV region, three sub-regions were identified. The epicardial layer (Epi) was defined as a portion of the free wall from the epicardium to the mid-wall. The remaining free wall inclusive of the endocardium was considered as the endocardial layer (Endo). The septal region (Sep) included a portion of the septum within each respective region. In Figure 3B, the PI accumulations identified in Epi and Endo of the aLV region and in Sep of the pLV region are shown. The ventricular cross-sections were divided into relatively simplified regions in order to reflect physiologically distinctive structures. During shock delivery, the extent of PI accumulation in the aRV region was large due to its close proximity to the shock electrode. No sub-distinction was made in this region, and it was collectively considered as the shock electrode region. PI-stained tissue volumes in all 4 regions of the transverse sections were summed over the entire ventricles to yield the overall electroporated tissue volume.

2.5 Histology

The transverse sections used in the fluorescence study were stained using Masson's trichrome (American MasterTech, Lodi, CA) for correlation of PI staining with structural changes. Histology images were captured by Retiga-SRV Fast 1394 camera (Q-Imaging, Surrey, British Columbia, Canada) on Leica DM5000B microscope (5X

objective) with 1.28 μm/pixel resolution. A motorized stage (H101 ProScan, Prior Scientific) controlled via Turboscan software (Objective Imaging, Kansasville, WI) running in Image-Pro enabled mosaic imaging of the entire cross-section (Figure 4). Muscle (red) and fibrous MI scar tissue (blue) areas were quantified in an automated fashion using Image-Pro. Infarct size was expressed as a percentage of the fibrous tissue volume with respect to the whole left and right ventricular tissue volume (Figure 5).

2.6 Statistical Analysis

Summary group data are reported as mean ± standard deviation. Statistical comparisons between two groups were performed using two-tailed, unpaired Student's *t*-Tests. Differences were considered significant when $p < 0.05$.

3. RESULTS

3. 1 Myocardial Infarction in the Ventricles

Masson's trichrome staining confirmed the location and extent of MI in the ventricles, as shown in Figure 4. Control hearts (top panel, Figure 4) were mostly stained in red for muscle tissue. In the MI heart (bottom panel, Figure 4), loss of myocardium led to thinning of the free wall and fibrous scar tissue formation[53] (blue). The MI was always mostly transmural in the LV free wall and mainly confined in the anterior LV free wall, extending toward the lateral and posterior LV free wall. In the infarcted free walls of all 7 MI hearts, both endocardial and epicardial BZs were observed. The endocardial BZ was always found as a relatively thick layer of surviving myocytes, lining the endocardium. In the epicardium, a thin layer or islands of surviving myocytes was infiltrated by fibrous scar tissue. Figure 5 shows spatial quantification of the fibrous tissue content along the long axis of the heart. The fibrous infarct scar was mainly in the apical region. The infarct volume was 13.8 ± 5.0% (n = 7) of the whole ventricles. An MI heart preparation in the perfusion chamber is shown in Figure 1.

3.2 Spatial Characterization of Electroporation in the Structurally Normal Hearts

First, the spatial distribution and extent of electroporation were characterized in the control hearts (Figure 6). In the control group without shock, there was no noticeable PI accumulation (top panel, Figure 6A). When a shock (+300-V, 8-ms monophasic) was delivered, electroporation was evident, especially in the shock electrode (SE) region (bottom panel, Figure 6A). The shock electrode and reference electrode (RE) positions

are illustratively indicated in one fluorescence image. The histology images of the same transverse sections are shown in the top panel of Figure 4. In all 5 hearts with shock, the extent of electroporation in the shock electrode region (gray traces, Figure 6B) was closely related to the location and dimension of the active region of the shock electrode along the long axis. At the very apex near the inactive region of the shock electrode, there was virtually no PI accumulation. Within the range spatially corresponding to the location of the active region, approximately 6 to 16 mm from the apex, electroporation was maximal. Total tissue area represents ventricular tissue area in the transverse sections (black traces). The circle markers indicate measurements made from the transverse sections shown in the bottom panel of Figure 6A. In all 5 control hearts with shock, electroporation always reached a transmural level in the anterior RV free wall (wall thickness: 2.2 ± 0.3 mm). In the septum, PI staining was transseptal in 2 hearts. The average depth of PI staining in 5 hearts was 60.9 ± 35.9% of the septum thickness (6.0 ± 2.9 mm).

The regional and overall extents of electroporation are summarized in Figure 6C. When no shock was delivered in control hearts (striped gray), there was little PI accumulation. In the control hearts with shock (solid gray), the extent of electroporation was most apparent in the shock electrode region (SE) with 14-fold increase in PI accumulation compared to the control hearts without shock. Within the control group with shock, the shock electrode region was significantly more electroporated than all remaining regions ($p < 0.05$). In the pRV, aLV, and pLV regions, there were only minute PI-positive traces. The overall normalized PI-positive tissue volume was increased by 2-fold to 5.9 ± 1.1% in the control group compared to the control hearts without shock.

3.3 Spatial Characterization of Electroporation in the Chronically Infarcted Hearts

The spatial distribution and extent of electroporation was similarly characterized in the MI hearts (Figure 7). As in the control group without shock, there was little PI accumulation in the MI hearts (top panel, Figure 7A) when no shock was delivered. Shock-induced electroporation was apparent in the MI group with shock (bottom panel, Figure 7A), similarly to the control group with shock. However, PI-staining of the aLV Epi region was different from the control group with shock (bottom panel, Figure 6A) and from the MI group without shock (top panel, Figure 7A). The same series of transverse sections are also shown in the bottom panel of Figure 4 for histological correlation. The characteristic dependence of electroporation parallel to the shock electrode was similar to the control hearts with shock (Figure 7B). In all 5 MI hearts with shock, the PI staining was also transmural in the anterior RV free wall (wall thickness: 2.6 ± 0.3 mm). In the septum (septum thickness: 6.4 ± 0.7 mm), the average depth of electroporation in 5 hearts was 67.0 ± 30.1%. Electroporation was transseptal in two hearts. There was no statistical difference ($p = 0.78$) in the depth of electroporation in the septum between the control (n = 5) and MI (n = 5) groups.

In Figure 7C, the regional and overall extent of electroporation in the MI hearts are summarized. When no shock was delivered, there was virtually no PI accumulation in the MI hearts (striped black). With shock delivery (solid black), the most substantial increase (22-fold) was found in the shock electrode region ($p < 0.05$ versus all remaining regions within the MI group with shock), similarly to the control group with shock. In the MI group with shock, however, there was a 27-fold increase in %PI Volume in the

epicardial layer of the aLV region. The overall %PI Volume was increased by 3-fold to 8.6 ± 2.6% in the MI group with shock compared to the MI hearts without shock.

The extent of electroporation in the control (n = 5, gray) and MI (n = 5, black) groups with shock was further compared in Figure 8. Electroporation in the shock electrode region ($p = 0.15$) as well as the overall extent of electroporation ($p = 0.07$) were similar between the control and MI groups with shock (Figure 8A). The aLV Epi region was more vulnerable to shock-induced electroporation in the MI hearts (*, $p < 0.05$). Comparison of raw tissue volumes (mm^3) before normalization confirmed that this difference was independent of heart size (Figure 8B). There was no significant difference ($p = 0.28$) in the total ventricular tissue volume. The overall PI-accumulated tissue volume in the control and MI groups with shock was also similar ($p = 0.17$). There was, however, significantly ($p < 0.05$) increased PI accumulation in the aLV Epi region of the MI group with shock (banded black) compared to the corresponding region of the control group with shock (banded gray).

Finally, to structurally correlate the heightened susceptibility to shock-induced electroporation in the aLV Epi region, fluorescence and histology images from 5 MI hearts with shock were compared. In Figure 9, a representative histology image of an MI transverse section is shown in the left column. Higher magnification images from the epicardial layer (red box) and the endocardial layer (green box) are shown in the right column along with the fluorescence images. In all MI hearts with shock, PI accumulation was observed only in a thin epicardial layer (red box) occupied by islands of surviving myocytes in the epicardial BZ. The surviving myocyte layer in the relatively thick endocardial BZ (green box), however, was not stained with PI.

4. CONCLUSION

4.1 Discussion

In this study, three key observations were made: 1) shock-induced electroporation was closely dependent transversely on the location and longitudinally on the dimension of the active region of the shock electrode; 2) upon one strong internal defibrillation shock delivery from the RV, the surviving epicardial layer of the infarcted region in the LV free wall was more susceptible to shock-induced electroporation; 3) the overall vulnerability to shock, however, was comparable between the control and MI groups. These findings partially reject the proposed hypothesis that MI hearts may be generally more susceptible to shock-induced electroporation. On the other hand, the heightened susceptibility of the surviving myocytes in the infarcted region of MI hearts to electroporation partially confirms the hypothesis.

In both structurally normal and chronically infarcted rabbit hearts, the most extensive electroporation was confined to the area near the defibrillation shock electrode. This may be due to the strong transmembrane polarization of cardiac tissue induced near the site of a strong electrical field gradient.[3] This finding can be further evidenced from the apex-to-base spatial dependence of electroporation with respect to the length of the active region of the shock electrode. The spatial distribution of electroporation correlated well with the position and dimension of the shock electrode. The occurrence of electroporation was confirmed to be a mid- or post-shock event, as there was virtually no accumulation of PI within tissue when no shock was delivered in the equivalent experimental setup.

In MI hearts (n = 5), electroporation in the aLV Epi region was significantly increased ($p < 0.05$) compared to the corresponding region in control hearts (n = 5). Passive diffusion of PI into the surviving myocytes in the BZ could not explain this finding because little PI accumulation occurred in this region of MI hearts when no shock was delivered. Membrane rupture of the surviving myocytes in the BZ may be more easily inducible by the shock application. The pathophysiologic conditions of the surviving myocytes appear not to be the sole cause of this increased vulnerability to electroporation because the surviving myocytes in the relatively thick endocardial BZ of aLV were not electroporated. Rather, remodeling of the surviving myocytes, thin layer of epicardial BZ, and structural heterogeneity of the BZ may be jointly attributed to the cause of heightened electroporation in the aLV Epi region. Increased structural heterogeneity[38] as well as disrupted electrical continuity[54, 55] by gap junction deorientation of the BZ may promote the development of a strong electrical field gradient in the far field.[37, 39, 56] The higher pathway resistance in the MI hearts during the shock delivery may indicate contribution of structural heterogeneity in the development of an electrical field gradient in the MI heart. The added contribution of the tissue-bath interface effect[3, 42, 57] may further induce a sufficient transmembrane polarization for the occurrence of electroporation. Al-Khadra *et al*.[3] reported that the endocardium was more susceptible to electroporation. However, it is difficult to correlate these two studies because an internal shock was delivered in the intact heart in this study as opposed to an external shock applied to a dissected tissue preparation in the earlier report. The myocardial structure and electrophysiology of the MI hearts in this study are also different from those of the normal heart used in the study by Al-Khadra *et al*.

The extent of electroporation was substantially larger in the shock electrode region than in the aLV Epi region. Thus, despite significantly increased electroporation in the aLV Epi region of MI hearts, the difference in the overall extent of electroporation between the control and MI groups did not reach a statistical significance. It was observed during fluorescence imaging that the infarcted region in MI hearts was visually less autofluorescent than the non-infarcted region. The average total ventricular myocardium volume in MI hearts (3044.62 ± 502.61 mm^3; n = 7) tended to be smaller (p = 0.08) than in control hearts (3650.20 ± 674.95 mm^3; n = 7). It was not, however, solely due to loss of myocardium to infarction. The difference in total ventricular tissue volume obtained from histological staining between the control (4054.68 ± 628.75 mm^3; n = 7) and MI (3825.97 ± 573.82 mm^3; n = 7) groups was smaller (p = 0.49). Following normalization by the histological total tissue volume in the control (n = 5) and MI (n = 5) groups with shock, the statistical comparison of the overall extent of electroporation resulted in p = 0.12. The extent of electroporation remained significantly larger ($p < 0.05$) in the aLV Epi region of the MI hearts with shock.

The increased vulnerability of the surviving myocytes in the infarcted region to shock-induced electroporation may play a significant role in defibrillation because the infarct BZ is known to provide a substrate for the origin and maintenance of sustained reentrant arrhythmia. In determining defibrillation failure or success, the significance of electroporation may lie in its spatial distribution and its effects on postshock cardiac electrical activity. Although electroporation may be bipolar in nature, one of pro- or anti-arrhythmogenic aspects may be emphasized in a greater degree depending on the extent of electroporation. Complete conduction block in the infarct BZ due to electroporation

may eliminate a proarrhythmogenic substrate for reentrant arrhythmia. On the contrary, partial conduction block in the infarcted BZ may accentuate the reentrant foci. In designing a more efficient defibrillation therapy, the spatially dependent distribution and extent of electroporation may need to be considered to minimize its antagonistic role in defibrillation. The spatial distribution of electroporation in the presence of infarct scar tissue provided in this study may be also a helpful tool in designing a systematic way of introducing gene or drug to a specific area within the heart that is more vulnerable to an electrical shock.

4.2 Study Limitations

In this study, a single +300-V, 8-ms truncated exponential monophasic shock was delivered in the paced heart. This relatively high shock intensity and positive polarity were chosen to facilitate characterization of electroporation while still clinically relevant.[3, 58] In order to address the limitations of this study and further characterize electroporation in the intact heart, in the future we plan to investigate 1) shock-intensity dependent, 2) shock-number and frequency dependent, and 3) shock-waveform dependent distribution and extent of electroporation. In addition, delivery of defibrillation shocks in the fibrillating heart would characterize electroporation during more clinically resembling defibrillation. A computer simulation would further enable correlation of experimentally quantified spatial distribution and extent of electroporation to the electrical field gradient within the intact heart model. In this study, electroporation in the infarct region may have been underestimated compared to clinical events because the

infarct was mainly in the LV free wall while transseptal MI is often observed in human patients.

4.3 Future Directions

In order to further investigate the vulnerability of the infarcted region to electroporation, the shock electrode was also previously inserted in LV. The spatial distribution of electroporation, however, varied largely among the hearts because it was difficult to reliably estimate the shock electrode position. In RV, the relatively small cavity restricted free movements of the shock electrode once it was positioned against the anterior free wall and the septum. The coil electrode, however, appeared bended or slanted in LV due to its larger cavity size. As a result, electroporation was found in the posterior LV free wall and the septum or in the lateral LV free wall and the septum potentially depending on the orientation of the shock electrode. In another approach, it was tried to create a transseptal LV MI in rabbits. In addition to ligating the lateral or posterolateral division, ligation of the left circumflex artery (LCX) was sought. LCX was not, however, always visible from the epicardial surface of the heart, and ligation of LCX did not systematically produce a transseptal MI. Alternatively, a stronger shock may be delivered from RV to investigate the spatial distribution and extent of electroporation in the infarcted region of LV.

Although the 300-V shock induced a quantifiable electroporation in the epicardial layer of the infarcted region, this shock intensity may not have been sufficient to elucidate the spatial dependence of electroporation in aLV Epi along the active region of the shock electrode. Whereas electroporation in the shock electrode region was found

closely related to the dimension of the active region, no clear spatial correlation could be observed in the aLV Epi region (Figure 10). In some MI hearts, nevertheless, it appeared electroporation was more pronounced at sites spatially corresponding to the edges of the active region of the shock electrode. In addition, the extent of electroporation appeared to be actually smaller in the midrange of the active region, contrary to the maximal electroporation of the SE region observed in this range. No qualitative or quantitative analysis could be performed at this point. The application of a very strong 500-V shock may generate a larger electrical gradient in the infarcted region. This approach, therefore, may experimentally relate the spatial distribution of electroporation in the infarcted region to the dimension of the active region of the shock electrode.

On the other hand, the 300-V shock used in this study always induced a large, transmural electroporation in the shock electrode region. This large electroporation may represent a complete, or saturated, electroporation of tissue within the pathway of electrical field. Even if MI hearts were more susceptible to electroporation than control hearts, consequently, it may not be fully reflected because all tissue available for electroporation in the shock electrode region may be totally electroporated. Occurrences of transseptal electroporation further corroborate this potentially saturated electroporation. In the infarcted region, moreover, the quantity of electroporated tissue was very small compared to the electroporated tissue quantity in the shock electrode region. As a result, despite the heightened vulnerability of the infarcted region to electroporation, its contribution to the overall extent of electroporation did not lead to a statistical significance. In order to further investigate the vulnerability of MI hearts to electroporation, shocks with lower intensities may be delivered. First, electroporation

may or may not be transmural and transseptal. The depth of electroporation penetrating the free wall and the septum may reveal differences in the vulnerability to electroporation between control and MI hearts. In addition, the overall extent of electroporation may better reflect shock-intensity dependence of electroporation.

In MI hearts, it is not known at what intensity of shock delivered from RV may result in electroporation of the infarcted region. This electroporation threshold may be lower than the defibrillation threshold. Although the 300-V shock used in this study did not induce postshock arrhythmia, it is also possible post-electroporation cardiac electrical activity may induce arrhythmia when shocks of different intensity are delivered. The shock intensities of 50 and 150 V in rabbit hearts may be of interest to investigate regarding the effect as well as the spatial distribution and extent of electroporation in both control and MI groups.

Multiple monophasic shocks of the same intensity or a biphasic shock may be delivered to characterize electroporation. In choosing appropriate shock intensities for multiple monophasic shocks or a biphasic shock, it is necessary to investigate the shock-intensity dependence of electroporation. In addition, the spatial distribution and extent of electroporation during successful event of defibrillation may be of paramount relevance in understanding the role of electroporation in defibrillation. First, arrhythmia can be induced in MI hearts by delivering a low-intensity shock during the vulnerable window.[58] While perfused with 30-μm PI-containing Tyrode solution, a rescue shock may be delivered to terminate arrhythmia. During fibrillation, however, the heart may possibly become more permeable to PI if the myocytes are subjected to ischemia. In the past, although not fibrillating, an ischemic heart was stained with PI throughout the septum

and the posterior RV and LV free walls even when no shock was delivered. It would be therefore necessary to find a means of prohibiting ischemia in the myocytes when inducing fibrillation. In studying the spatial and extent of electroporation, the current methods of data collection and analysis can be used to quantify regional and overall PI-accumulation in the transverse sections.

Recently, methods of investigating connexin 43 (Cx43) redistribution following electroporating shock were developed. Western blot analysis and immunohistochemical staining quantify the overall amount and spatial orientation, respectively, of Cx43 in its phosphorylated as well as dephosphorylated states. In combination with the spatial distribution of electroporation in the infarcted hearts, these may provide a more comprehensive understanding of the effects of postshock cardiac electrical activity in defibrillation.

FIGURES

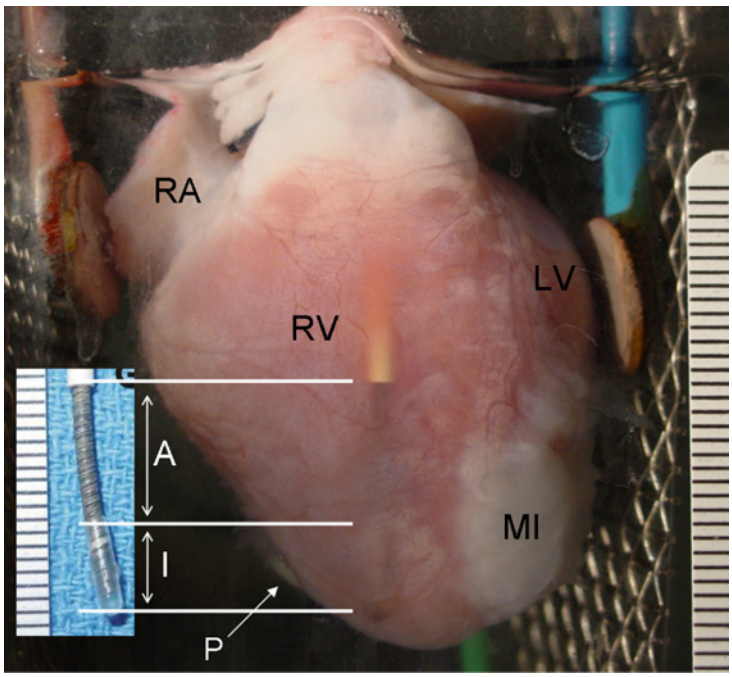

Figure 1. Heart preparation. An MI heart is shown. The shock electrode (SE) inserted in RV is visible through the anterior RV free wall. The distal tip of the shock electrode (inset) was composed of a 6-mm nonconducting inactive region (I) and a 10-mm active region (A). The pacing electrode (P) was positioned at the apex of the posterior RV free wall. RA indicates the right atrium; RV, the right ventricle; LV, the left ventricle; MI, myocardial infarct.

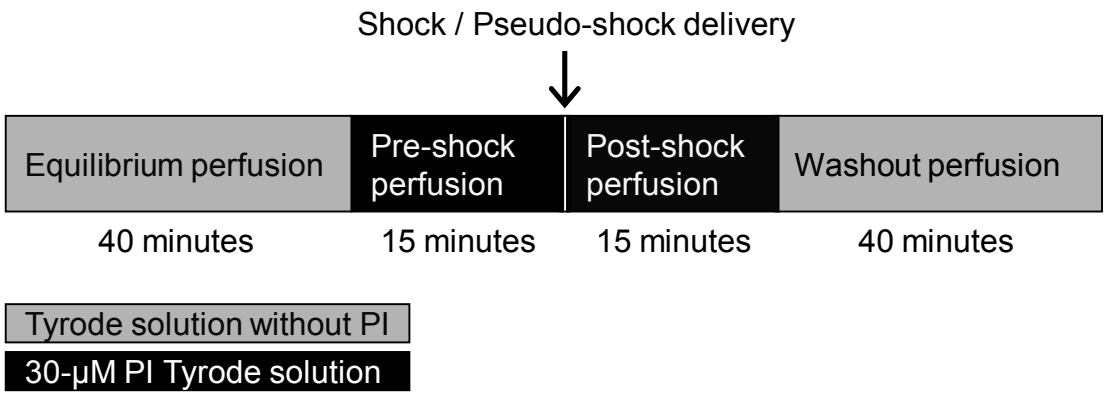

Figure 2. Diagram of experimental protocol. During equilibrium and washout perfusions, the heart was perfused with no-PI containing Tyrode solution. 15 minutes prior to and following shock or pseudo-shock delivery, the heart was perfused with 30-μM PI-containing Tyrode solution.

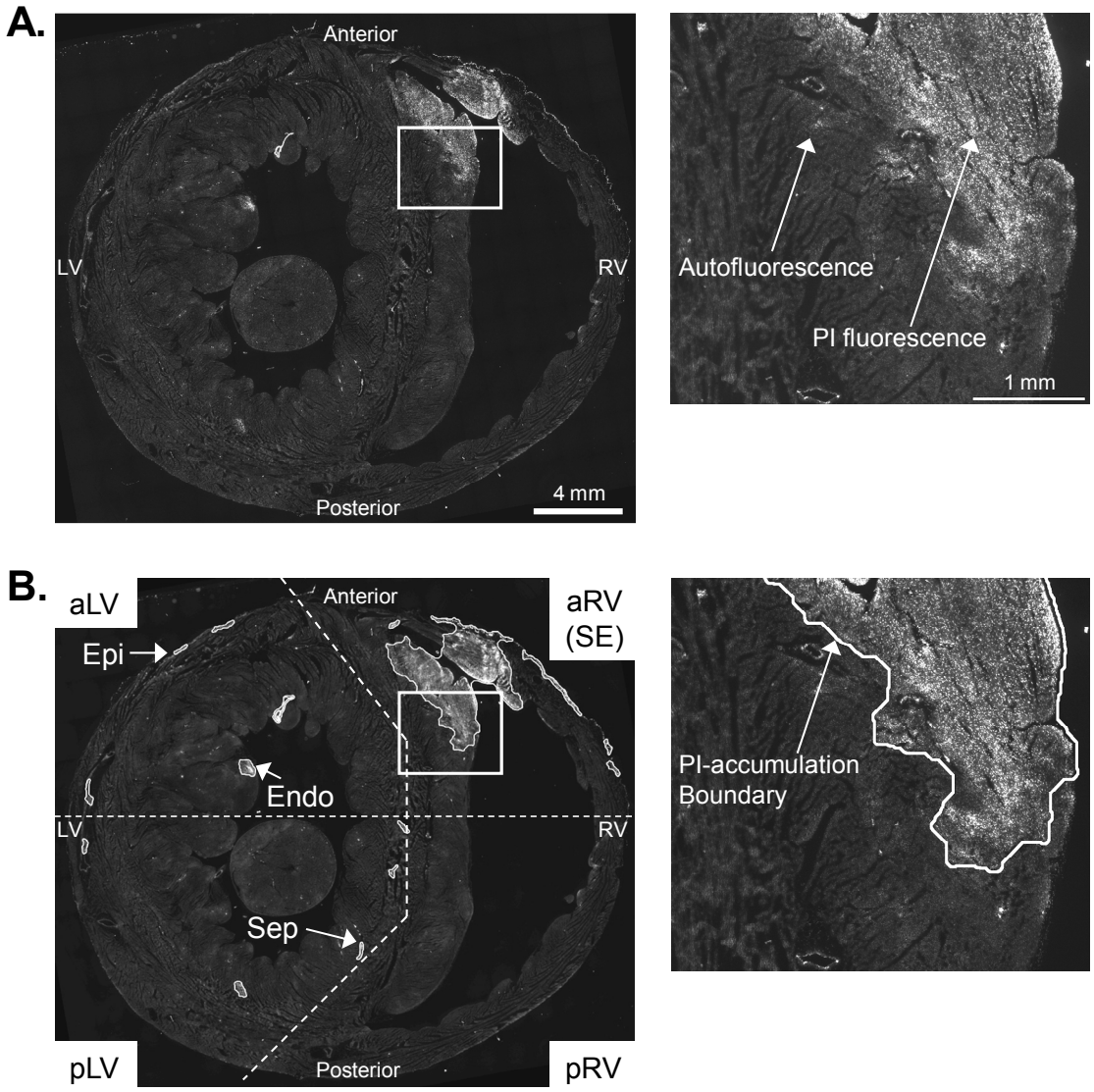

Figure 3. Identification of electroporated tissue area. After shock delivery, PI-stained nuclei appeared as bright fluorescence signal. The ventricular tissue is visible by autofluorescence. The right column shows a magnified view of the white box in the left column images. **A**. A raw mosaic image of the entire ventricular transverse section. **B**. The transverse section shown in **A** was processed for PI quantification. Clusters of PI-accumulated tissue were identified, and their boundaries were traced. PI-accumulations in the aLV Epi, aLV Endo, and pLV Sep regions are representatively indicated (refer to Methods for abbreviations).

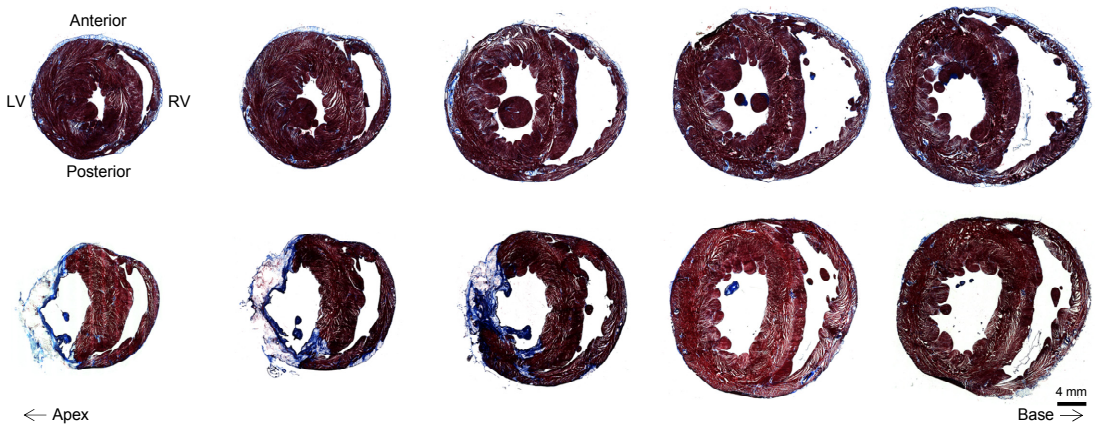

Figure 4. Histology. Transverse sections from the control (top panel) and MI (bottom panel) groups were stained by Masson's trichrome. Muscle was stained in red and fibrous scar tissue in blue. The series of sections are shown from the apex (left) toward the base (right). Fluorescence images of the same transverse sections are shown in the bottom panels of Figure 6A and Figure 7A, respectively.

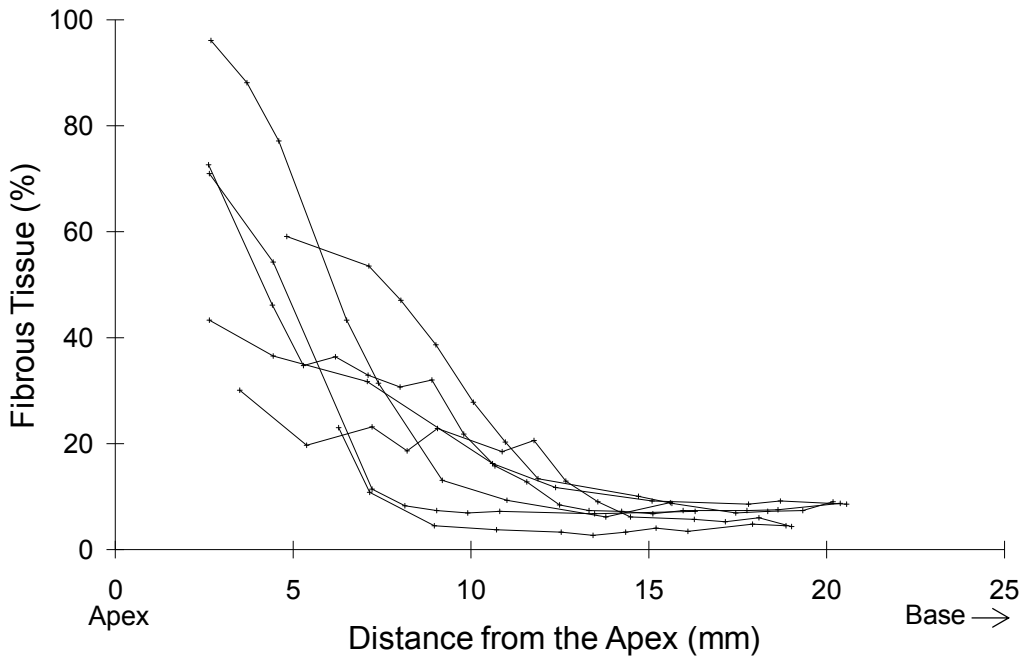

Figure 5. Spatial fibrous tissue content in MI hearts. Fibrous tissue content was quantified from the apex to the base along the long axis of MI hearts.

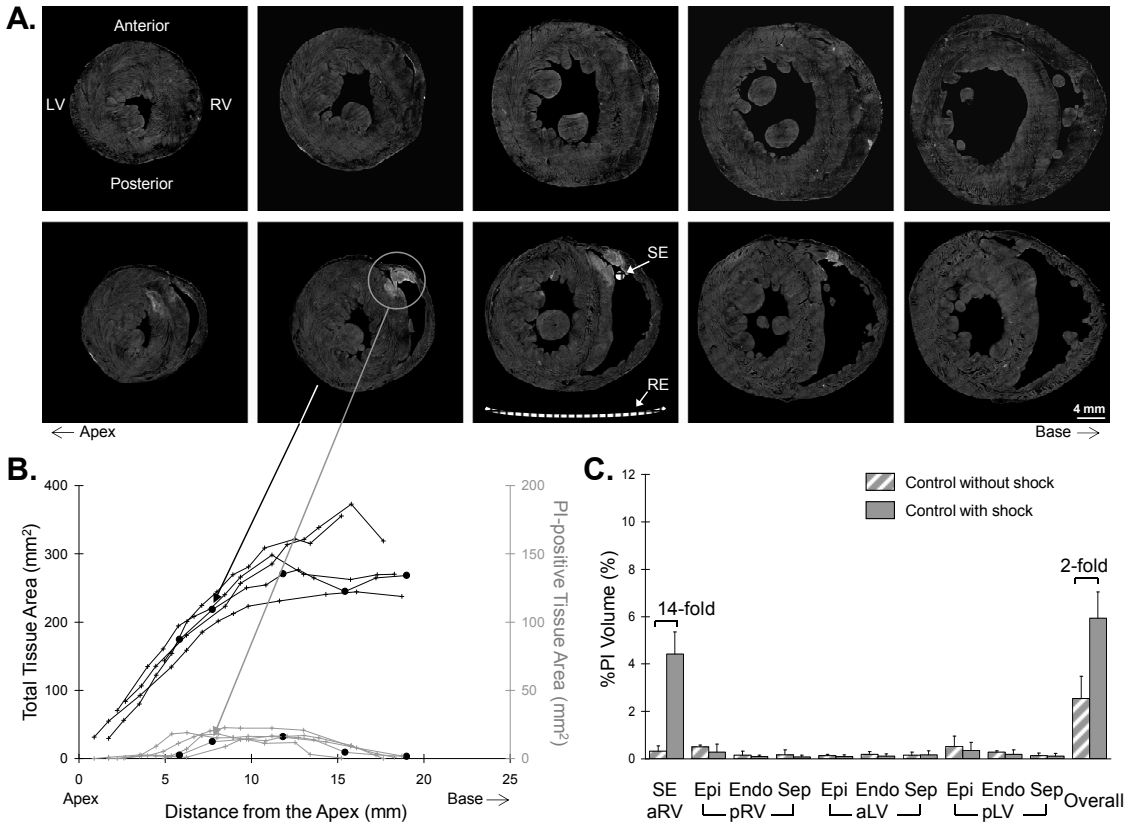

Figure 6. Spatial distribution and extent of electroporation in control hearts. **A**. Series of transverse sections from the control hearts without shock (top row) and with shock (bottom row). The shock electrode (SE) and reference electrode (RE) positions are representatively illustrated. **B**. Electroporation was quantified in the shock electrode region along the long axis of the heart. The circle markers indicate measurements of the total tissue (black) and PI-accumulated tissue (gray) areas from the sections shown in the bottom row of **A**. **C**. The regional and overall extent of electroporation in the control group was quantified by integrating the area measurements along the long axis.

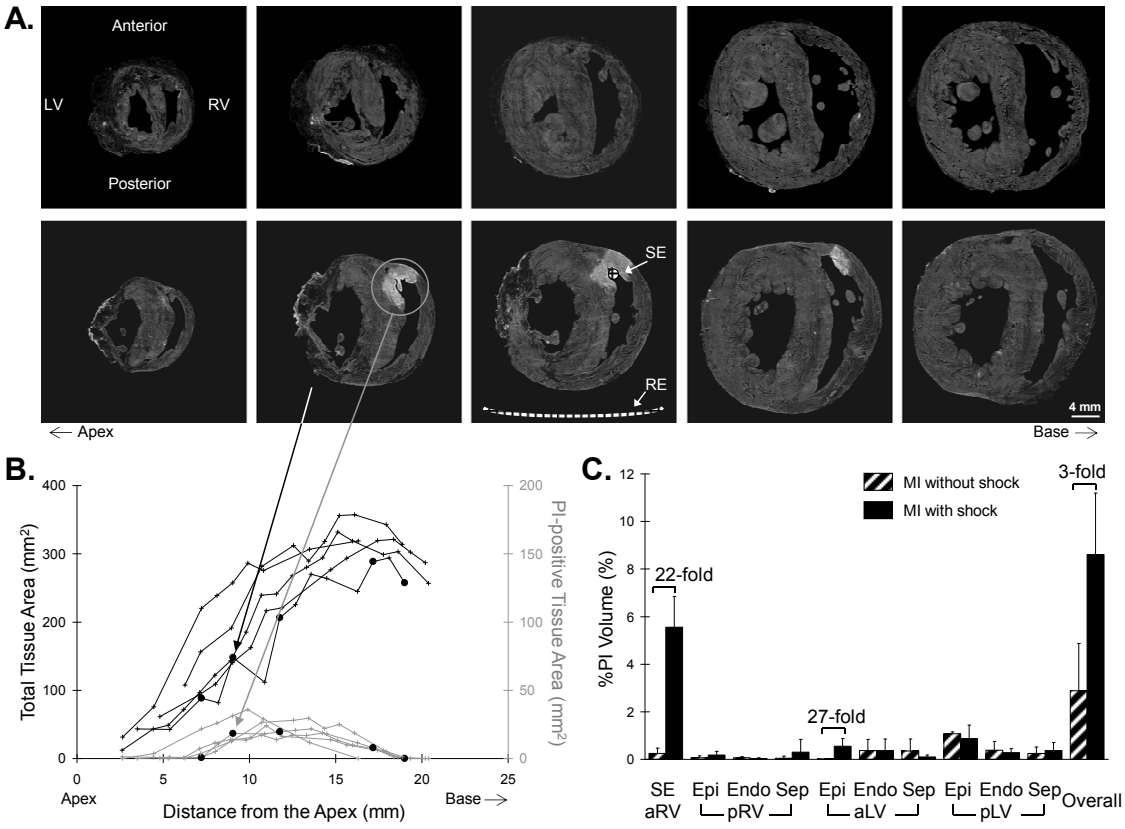

Figure 7. Spatial distribution and extent of electroporation in MI hearts. Refer to **Figure 3** legend for descriptions.

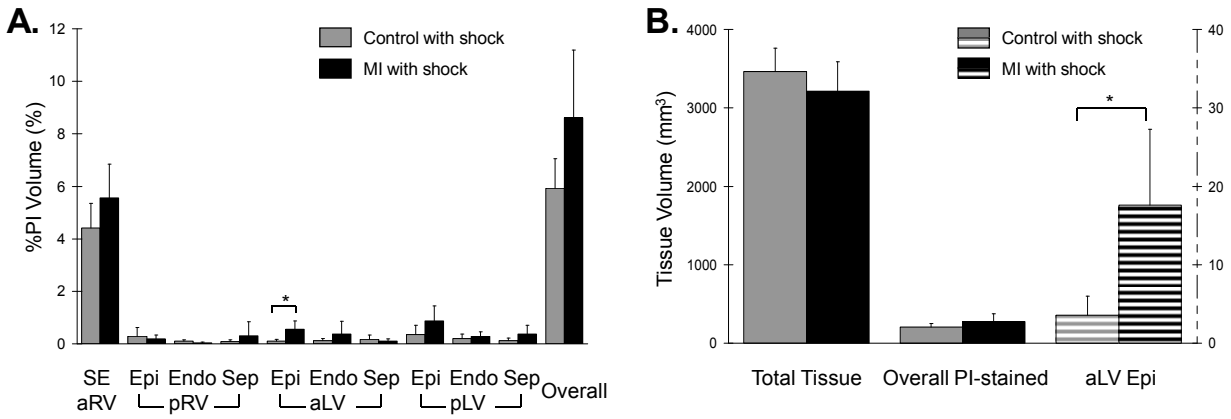

Figure 8. Electroporation in the control and MI groups with shock. **A**. The regional and overall extent of electroporation is compared between the control and MI groups with shock. **B**. Raw measurements of the ventricular myocardium volume (Total Tissue) as well as PI-accumulated tissue volumes in the entire ventricles (Overall PI-stained) and in the aLV Epi region (1/100 scale) before normalization. (*, $p < 0.05$)

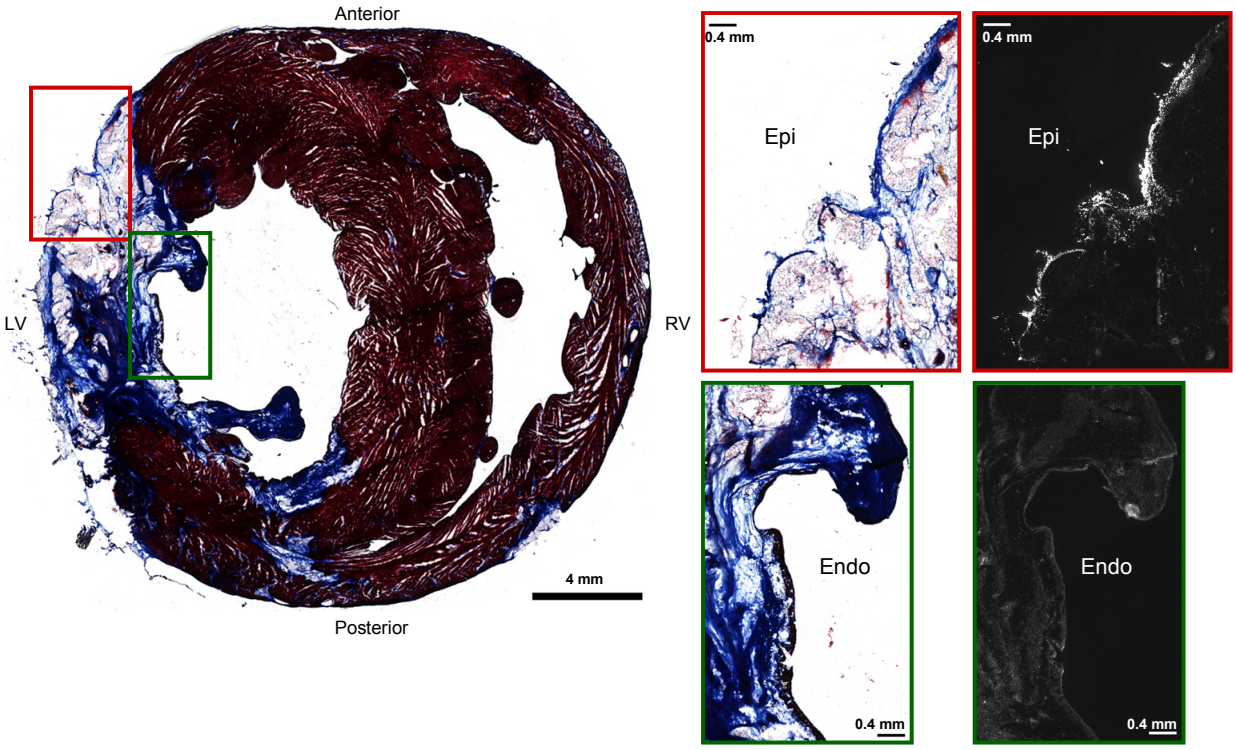

Figure 9. Structural correlation of the infarcted region. A histology image of an MI transverse section is shown in the left column. Higher magnification images from the epicardial layer (red box) and the endocardial layer (green box) are shown in the right column along with the fluorescence images in the same area. The same transverse section is shown in Figure 4 for histology (middle of the bottom panel) and in Figure 7A for PI fluorescence (middle of the bottom panel).

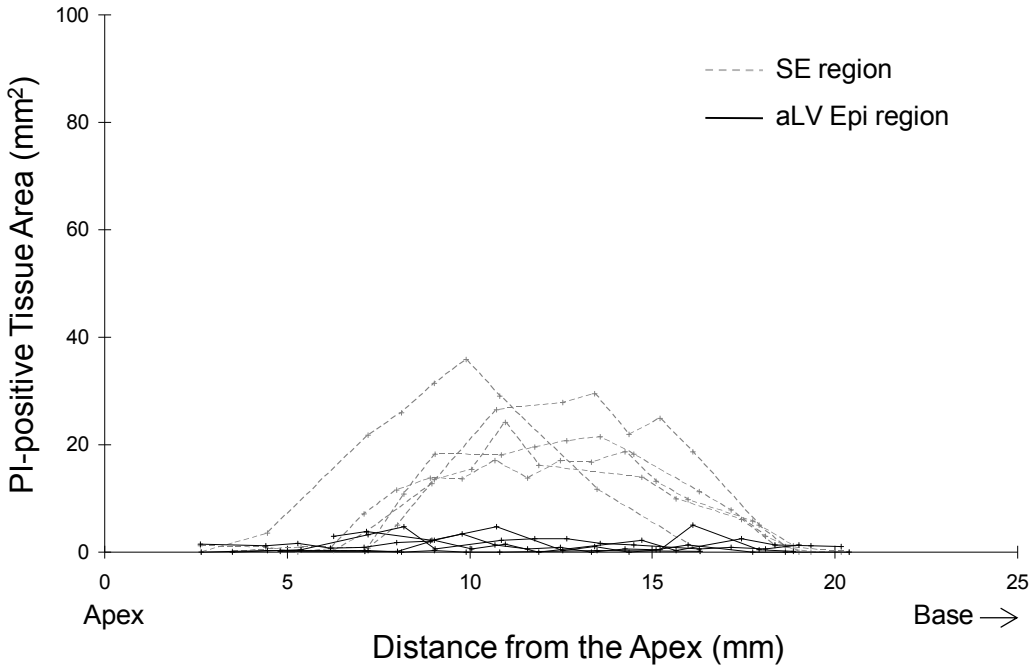

Figure 10. Electroporation in the epicardial layer of the infarcted region. The spatial extent of electroporation in the shock electrode (SE) region (dotted gray) and in the aLV Epi region (solid black) is shown along the long axis of the heart.

Appendix I: Extended Methods

Animal Model

Rabbits at the age of 115 ± 14 days were anesthetized by intramuscular injection of ketamine (35 mg/kg) and xylazine (5 mg/kg). An intravenous line was inserted trough the marginal ear vein, and the rabbits were intubated with Sheridan cuffed tracheal tube (3.0-mm inside diameter; Hudson RCI, Research Triangle Park, NC). The anesthesia was maintained by one to two percent isoflurane in oxygen. The rate of positive pressure-driven mechanical ventilation was adjusted according to the inspiration airway pressure and the carbon monoxide saturation level. Rabbits were kept warm on a water heated blanket at 38˚C whenever possible. Saline was continuously infused via the intravenous line. Upon opening the chest and the pericardium, a silk 5-0 surgical suture (Ethicon, Piscataway, NJ) was placed at the tip of the apex to orient the heart. The target artery was ligated with a polypropylene 5-0 surgical suture (Ethicon). The potential extent of infarction was confirmed and assessed by immediately visible myocardial cyanosis. Elevation of the ST-segment in ECG was also observed. Depending on the location and severity of the myocardial cyanosis, one or two more epicardial branches of the coronary artery that were visible were further ligated. The ribs were approximated by three evenly placed polyester 0 surgical sutures (Ethicon), and suture the suture layers were made using Ethicon polypropylene 2-0 sutures. The concentration of isoflurane gas was progressively reduced, and when voluntary breathing was restored, the tracheal tube was removed. An analgesic (Buprenex, 0.02 mg/kg) was injected intramuscularly.

Heart Preparation

Rabbits were anesthetized by a combination of pentobarbital sodium (50 mg/kg) and heparin (500-1000 USP Units/kg) through the ear vein. Heparin was used to inhibit coagulation of blood. A ventral incision was made with the rabbit in supine position. The heart was excised at the aortic arch level. The aorta was immediately cannulated and perfused with oxygenated modified Tyrode solution with the following concentrations (mM): NaCl, 128.20; $CaCl_2$, 1.30; KCl, 4.70; $MgCl_2$, 1.05; NaH_2PO_4, 1.19; $NaHCO_3$, 20.00; glucose, 11.11. The perfusion pressure was controlled and maintained within 20 to 60 mmHg range by the perfusion rate (mL/min). The heart was paced by a stimulus current of twice the diastolic pacing threshold and 2 ms in duration. A modified single lead electrocardiogram (ECG) was acquired by three Ag/AgCl plate electrodes placed in the perfusion chamber. Two leads are visible in Figure 1 while the green ground lead is not visible.

Experimental protocol

The timing of shock delivery was controlled by the custom-developed interface[51] designed in LabVIEW (National Instruments, Austin, TX). The shock was delivered 160 ms after the onset of immediately preceding pacing stimulus, during the repolarization phase of an action potential. The heart was continuously paced at the basic cycle length (300 ms) before and following shock delivery. In the control and MI groups without shock, shock delivery mechanism was not activated in the HVS-02 clinical defibrillator, and only a pseudo-shock was delivered while recording ECG. During washout, PI-

containing Tyrode solution was not returned back to the perfusion chamber. A new 2-μm filter was also used.

Sectioning of the ventricles from the apex to the base yielded 23 ± 4 transverse sections. At each cutting position, three 20-μm thick sections and two 10-μm thick sections were collected, from which only one 20-μm thick sections was used in this study.

Fluorescence study

11 ± 2 slides in control hearts and 12 ± 3 slides in MI hearts were visually selected for imaging from the collected samples. First, one 20-μm thick section from each cutting position was observed on the Leica epifluorescence microscope. Because the PI-positive fluorescence was most apparent near the shock electrode, slides of similar PI distribution pattern in this region were grouped together. At least one slide from each group was then imaged to represent the spatial dynamics of PI accumulation in the shock electrode region along the long axis of the heart. In order to ensure that the maximally electroporated tissue section was imaged and quantified, sections from immediately preceding and following cutting positions were additionally imaged and quantified. The slides were stored at -20˚C for three to five days before imaging in order to enhance detection of autofluorescence used for the ventricular myocardium area quantification. The camera exposure in the heart was determined by exploring and selecting the shutter open duration that was long enough for thresholding of the autofluorescence while minimizing pixel intensity saturation and leakage. The camera background was minimal, and no background correction was performed. In Image-Pro, the PI-accumulated tissue boundaries were traced from the Euclidian distance map of PI-stained nuclei. A macro is

written to automate this procedure as well as area quantifications and regional characterization. The macro also rejected systematically very small, yet visually identifiable PI accumulations in the endothelial lining of the coronary arteries. The thicknesses of the RV free wall and the septum along with respective depths of electroporation were measured by two-point Euclidian distance perpendicular to the free wall or septum orientation, respectively (Figure 11).

Histology

To histologically stain 20-μm thick sections, the staining protocol was optimized. Sections from the same heart were stained at once to minimize variation due to staining conditions. During histology imaging, the camera and microscope settings were kept constant for all hearts. White balancing and shading corrections were performed as needed. For tissue area quantification using a macro written in Image-Pro, the brightfield images in the RGB color space were first transformed into the YIQ color space. The areas of muscle tissue stained in red and MI scar stained in blue were then quantified from the in-phase channel. The sum of red and blue tissue areas was considered as the total ventricular tissue area. In a similar manner as in the fluorescence study, the fibrous and total tissue areas were spatially represented with respect to the apex, and the tissue volumes were integrated and estimated.

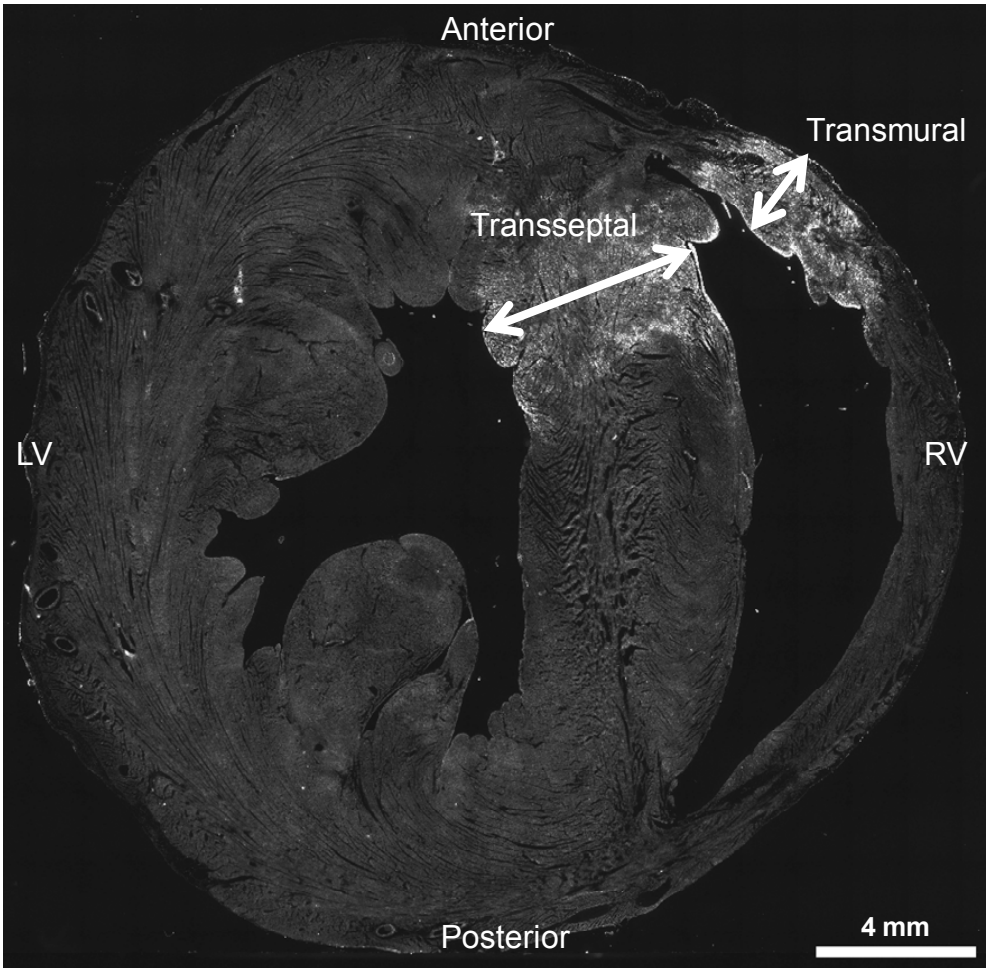

Figure 11. Free wall and septum thickness measurements. A representative transverse section with transseptal and transmural electroporation is shown.

Appendix II: Extended Results and Discussion

Infarct Size Measurement

The fibrous tissue content was quantified in both control (n = 7) and MI (n = 7) groups. In control hearts, a small quantity of collagenous matrix[59] was also stained in blue. It was mainly found as thin linings on the outer boundaries of the transverse sections and on the inner boundaries of the blood vessels as well as in the interstitial space. A similar pattern of fibrous tissue staining was also observed in the non-infarcted regions of MI hearts, but the fibrous tissue was visually larger and concentrated within the MI scar. In comparison to control hearts (5.7 ± 2.2%), the fibrous tissue content was significantly larger ($p < 0.05$) in MI hearts.

An area-based method may result in a smaller percentage value compared to the length-based method because loss of myocardium and thinning of the free wall following infarction reduce tissue area. The length-based method, in which the arc length of the infarct is measured with respect to the arc length of the free wall, may be more suitable in following the severity of postinfarct myocardium loss over a period of time. In the chronic model, however, the extent of infarction measured by both area-based and length-based method was well related to the cardiac function attenuation, as reported by Takagawa *et al*.[53] Although the length-based infarct size measurement may provide a better representation of progressive extent and severity of infarction, the area-based measurement estimates tissue area remaining in the infarcted heart. In lieu of quantifying electroporation in terms of tissue area accumulated with PI with respect to the total tissue

area, therefore, the area-based method is more relevant in this study because it quantifies tissue area available for electroporation.

Total Ventricular Myocardium Size

During fluorescence imaging, it was observed the infarcted region in the MI hearts was visually less autofluorescent than the non-infarcted region. As a result, the average total ventricular myocardium volume in the MI hearts (3044.62 ± 502.61 mm^3; n = 7) was smaller (p = 0.08) than in the control hearts (3650.20 ± 674.95 mm^3; n = 7). It was not, however, solely due to loss of myocardium to infarction. In the histologically stained total ventricular myocardium volumes, the difference (p = 0.49) between the control (4054.68 ± 628.75 mm^3; n = 7) and MI (3825.97 ± 573.82 mm^3; n = 7) groups was smaller (Figure 12), indicating the total tissue amount in the MI hearts was comparable to the control hearts despite infarction. The average non-fibrous tissue volume in the control group was, nevertheless, larger than in the MI group. Because the extent of electroporation was represented with respect to the autofluorescent total tissue volume, it appeared the non-significant increase (p = 0.07) in the overall extent of electroporation in the MI group with shock (n = 5) may be attributed to the underestimated total tissue volume. Following normalization by the histology total tissue volumes in the control and MI groups with shock, the statistical comparison of the overall extent of electroporation resulted in p = 0.12. The extent of electroporation remained significantly larger ($p < 0.05$) in the aLV Epi region of the MI hearts with shock.

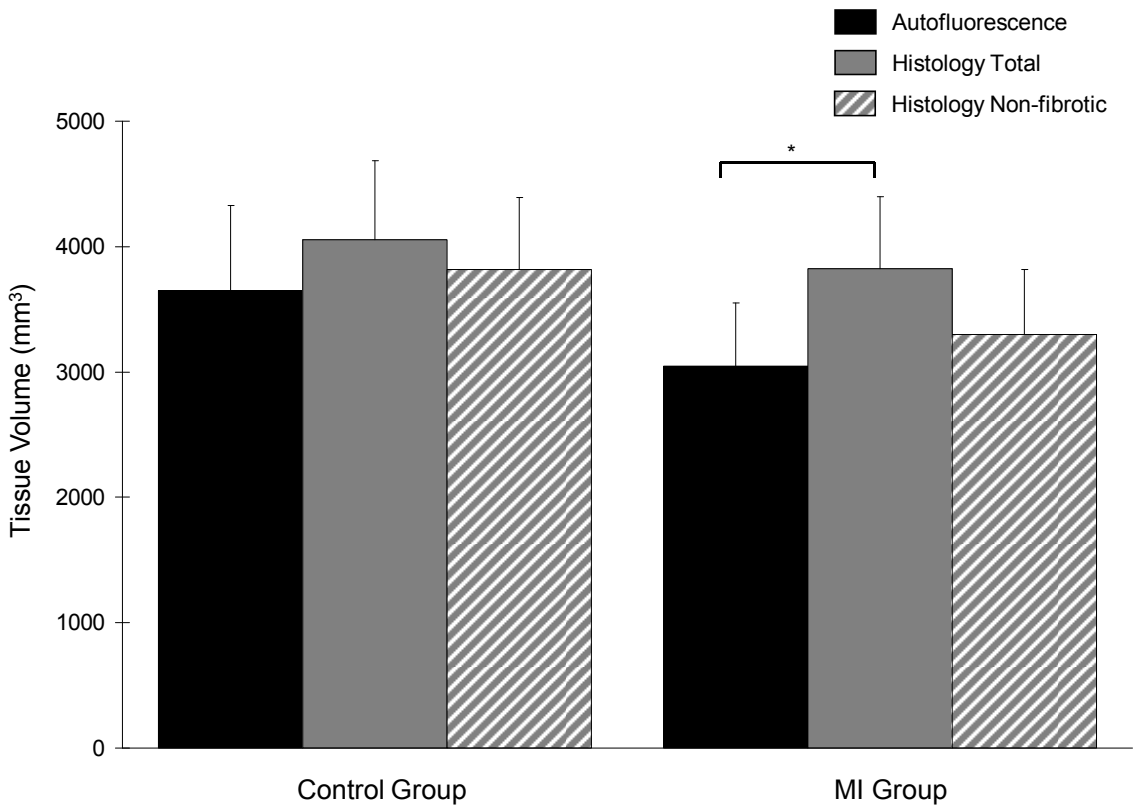

Figure 12. Comparison of ventricular myocardium volumes. The autofluorescent total ventricular tissue volume (black) was non-significantly smaller in the MI group compared to the control group. Histology total tissue volumes (solid gray) were more comparable between the control and MI groups. There was a significant difference (*, $p < 0.05$) between the autofluorescent and histology total tissue volumes in the MI group. Non-fibrous tissue volumes quantified by histology (striped gray) were more similar to the autofluorescent total tissue volumes both in control and MI groups.

References

1. Xie J, Weil MH, Sun S, Tang W, Sato Y, Jin X, Bisera J: High-energy defibrillation increases the severity of postresuscitation myocardial dysfunction. Circulation. 1997;96:683-688.

2. Sambelashvili AT, Nikolski VP, Efimov IR: Virtual electrode theory explains pacing threshold increase caused by cardiac tissue damage. Am J Physiol Heart Circ Physiol. 2004;286:H2183-2194.

3. Al-Khadra A, Nikolski V, Efimov IR: The role of electroporation in defibrillation. Circ Res. 2000;87:797-804.

4. Li L, Nikolski V, Wallick DW, Efimov IR, Cheng Y: Mechanisms of enhanced shock-induced arrhythmogenesis in the rabbit heart with healed myocardial infarction. Am J Physiol Heart Circ Physiol. 2005;289:H1054-1068.

5. Lee RC: Injury by electrical forces: pathophysiology, manifestations, and therapy. Curr Probl Surg. 1997;34:677-764.

6. Harrison RL, Byrne BJ, Tung L: Electroporation-mediated gene transfer in cardiac tissue. FEBS Lett. 1998;435:1-5.

7. Trollet C, Bloquel C, Scherman D, Bigey P: Electrotransfer into skeletal muscle for protein expression. Curr Gene Ther. 2006;6:561-578.

8. Weaver JC: Electroporation: a general phenomenon for manipulating cells and tissues. J Cell Biochem. 1993;51:426-435.

9. Jones JL, Jones RE, Balasky G: Microlesion formation in myocardial cells by high-intensity electric field stimulation. Am J Physiol. 1987;253:H480-486.

10. Cheng DK, Tung L, Sobie EA: Nonuniform responses of transmembrane potential during electric field stimulation of single cardiac cells. Am J Physiol. 1999;277:H351-362.

11. Knisley SB, Grant AO: Asymmetrical electrically induced injury of rabbit ventricular myocytes. J Mol Cell Cardiol. 1995;27:1111-1122.

12. Tovar O, Tung L: Electroporation and recovery of cardiac cell membrane with rectangular voltage pulses. Am J Physiol. 1992;263:H1128-1136.

13. Neunlist M, Tung L: Dose-dependent reduction of cardiac transmembrane potential by high-intensity electrical shocks. Am J Physiol. 1997;273:H2817-2825.

14. Aguel F, Debruin KA, Krassowska W, Trayanova NA: Effects of electroporation on the transmembrane potential distribution in a two-dimensional bidomain model of cardiac tissue. J Cardiovasc Electrophysiol. 1999;10:701-714.

15. DeBruin KA, Krassowska W: Electroporation and shock-induced transmembrane potential in a cardiac fiber during defibrillation strength shocks. Ann Biomed Eng. 1998;26:584-596.

16. Krauthamer V, Jones JL: Calcium dynamics in cultured heart cells exposed to defibrillator-type electric shocks. Life Sci. 1997;60:1977-1985.

17. Kodama I, Shibata N, Sakuma I, Mitsui K, Iida M, Suzuki R, Fukui Y, Hosoda S, Toyama J: Aftereffects of high-intensity DC stimulation on the electromechanical performance of ventricular muscle. Am J Physiol. 1994;267:H248-258.

18. Nikolski VP, Efimov IR: Electroporation of the heart. Europace. 2005;7 Suppl 2:146-154.

19. Janks DL, Roth BJ: Simulations of optical mapping during electroporation. Conf Proc IEEE Eng Med Biol Soc. 2004;5:3581-3584.

20. Ashihara T, Trayanova NA: Cell and tissue responses to electric shocks. Europace. 2005;7 Suppl 2:155-165.

21. Ashihara T, Yao T, Namba T, Ito M, Ikeda T, Kawase A, Toda S, Suzuki T, Inagaki M, Sugimachi M, Kinoshita M, Nakazawa K: Electroporation in a model of cardiac defibrillation. J Cardiovasc Electrophysiol. 2001;12:1393-1403.

22. Ohuchi K, Fukui Y, Sakuma I, Shibata N, Honjo H, Kodama I: A dynamic action potential model analysis of shock-induced aftereffects in ventricular muscle by reversible breakdown of cell membrane. IEEE Trans Biomed Eng. 2002;49:18-30.

23. Efimov IR, Gray RA, Roth BJ: Virtual electrodes and deexcitation: new insights into fibrillation induction and defibrillation. J Cardiovasc Electrophysiol. 2000;11:339-353.

24. Efimov IR, Cheng Y, Yamanouchi Y, Tchou PJ: Direct evidence of the role of virtual electrode-induced phase singularity in success and failure of defibrillation. J Cardiovasc Electrophysiol. 2000;11:861-868.

25. Efimov IR, Cheng Y, Van Wagoner DR, Mazgalev T, Tchou PJ: Virtual electrode-induced phase singularity: a basic mechanism of defibrillation failure. Circ Res. 1998;82:918-925.

26. Krassowska W: Effects of electroporation on transmembrane potential induced by defibrillation shocks. Pacing Clin Electrophysiol. 1995;18:1644-1660.

27. Janse MJ, Wit AL: Electrophysiological mechanisms of ventricular arrhythmias resulting from myocardial ischemia and infarction. Physiol Rev. 1989;69:1049-1169.

28. Downar E, Saito J, Doig JC, Chen TC, Sevaptsidis E, Masse S, Kimber S, Mickleborough L, Harris L: Endocardial mapping of ventricular tachycardia in the intact human ventricle. III. Evidence of multiuse reentry with spontaneous and induced block in portions of reentrant path complex. J Am Coll Cardiol. 1995;25:1591-1600.

29. Misier AR, Opthof T, van Hemel NM, Vermeulen JT, de Bakker JM, Defauw JJ, van Capelle FJ, Janse MJ: Dispersion of 'refractoriness' in noninfarcted myocardium of patients with ventricular tachycardia or ventricular fibrillation after myocardial infarction. Circulation. 1995;91:2566-2572.

30. El-Sherif N, Hope RR, Scherlag BJ, Lazzara R: Re-entrant ventricular arrhythmias in the late myocardial infarction period. 2. Patterns of initiation and termination of re-entry. Circulation. 1977;55:702-719.

31. El-Sherif N, Scherlag BJ, Lazzara R, Hope RR: Re-entrant ventricular arrhythmias in the late myocardial infarction period. 1. Conduction characteristics in the infarction zone. Circulation. 1977;55:686-702.

32. Peters NS, Coromilas J, Severs NJ, Wit AL: Disturbed connexin43 gap junction distribution correlates with the location of reentrant circuits in the epicardial border zone of healing canine infarcts that cause ventricular tachycardia. Circulation. 1997;95:988-996.

33. Wit AL, Dillon SM, Coromilas J, Saltman AE, Waldecker B: Anisotropic reentry in the epicardial border zone of myocardial infarcts. Ann N Y Acad Sci. 1990;591:86-108.

34. Wit AL, Janse MJ: Experimental models of ventricular tachycardia and fibrillation caused by ischemia and infarction. Circulation. 1992;85:I32-42.

35. Frazier DW, Wolf PD, Wharton JM, Tang AS, Smith WM, Ideker RE: Stimulus-induced critical point. Mechanism for electrical initiation of reentry in normal canine myocardium. J Clin Invest. 1989;83:1039-1052.

36. Zipes DP, Fischer J, King RM, Nicoll Ad, Jolly WW: Termination of ventricular fibrillation in dogs by depolarizing a critical amount of myocardium. Am J Cardiol. 1975;36:37-44.

37. Fishler MG: Syncytial heterogeneity as a mechanism underlying cardiac far-field stimulation during defibrillation-level shocks. J Cardiovasc Electrophysiol. 1998;9:384-394.

38. Hooks DA, Tomlinson KA, Marsden SG, LeGrice IJ, Smaill BH, Pullan AJ, Hunter PJ: Cardiac microstructure: implications for electrical propagation and defibrillation in the heart. Circ Res. 2002;91:331-338.

39. Sobie EA, Susil RC, Tung L: A generalized activating function for predicting virtual electrodes in cardiac tissue. Biophys J. 1997;73:1410-1423.

40. Fast VG, Rohr S, Gillis AM, Kleber AG: Activation of cardiac tissue by extracellular electrical shocks: formation of 'secondary sources' at intercellular clefts in monolayers of cultured myocytes. Circ Res. 1998;82:375-385.

41. Trayanova N, Skouibine K, Aguel F: The role of cardiac tissue structure in defibrillation. Chaos. 1998;8:221-233.

42. Entcheva E, Eason J, Efimov IR, Cheng Y, Malkin R, Claydon F: Virtual electrode effects in transvenous defibrillation-modulation by structure and interface: evidence from bidomain simulations and optical mapping. J Cardiovasc Electrophysiol. 1998;9:949-961.

43. White JB, Walcott GP, Pollard AE, Ideker RE: Myocardial discontinuities: a substrate for producing virtual electrodes that directly excite the myocardium by shocks. Circulation. 1998;97:1738-1745.

44. Cheek ER, Fast VG: Nonlinear changes of transmembrane potential during electrical shocks: role of membrane electroporation. Circ Res. 2004;94:208-214.

45. Nikolski VP, Sambelashvili AT, Krinsky VI, Efimov IR: Effects of electroporation on optically recorded transmembrane potential responses to high-intensity electrical shocks. Am J Physiol Heart Circ Physiol. 2004;286:H412-418.

46. Tsong TY: Electroporation of cell membranes. Biophys J. 1991;60:297-306.

47. Lavee J, Onik G, Mikus P, Rubinsky B: A novel nonthermal energy source for surgical epicardial atrial ablation: irreversible electroporation. Heart Surg Forum. 2007;10:E162-167.

48. Ootaki Y, Yamada H, Daimon M, Kamohara K, Popovic Z, Van Wagoner DR, Cheng Y, Fukamachi K: An experimental rabbit model for off-pump left ventricular reconstruction following left ventricular aneurysm. Heart Surg Forum. 2006;9:E786-791.

49. Podesser B, Wollenek G, Seitelberger R, Siegel H, Wolner E, Firbas W, Tschabitscher M: Epicardial branches of the coronary arteries and their distribution in the rabbit heart: the rabbit heart as a model of regional ischemia. Anat Rec. 1997;247:521-527.

50. Lee BH, Kim WH, Choi MJ, Rho JR, Kim WG: Chronic heart failure model in rabbits based on the concept of the bifurcation/trifurcation coronary artery branching pattern. Artif Organs. 2002;26:360-365.

51. Efimov IR, Cheng YN, Biermann M, Van Wagoner DR, Mazgalev TN, Tchou PJ: Transmembrane voltage changes produced by real and virtual electrodes during monophasic defibrillation shock delivered by an implantable electrode. J Cardiovasc Electrophysiol. 1997;8:1031-1045.

52. Cheng Y, Mowrey KA, Nikolski V, Tchou PJ, Efimov IR: Mechanisms of shock-induced arrhythmogenesis during acute global ischemia. Am J Physiol Heart Circ Physiol. 2002;282:H2141-2151.

53. Takagawa J, Zhang Y, Wong ML, Sievers RE, Kapasi NK, Wang Y, Yeghiazarians Y, Lee RJ, Grossman W, Springer ML: Myocardial infarct size measurement in the mouse chronic infarction model: comparison of area- and length-based approaches. J Appl Physiol. 2007;102:2104-2111.

54. Nassif G, Dillon SM, Rayhill S, Wit AL: Reentrant circuits and the effects of heptanol in a rabbit model of infarction with a uniform anisotropic epicardial border zone. J Cardiovasc Electrophysiol. 1993;4:112-133.

55. Dillon SM, Allessie MA, Ursell PC, Wit AL: Influences of anisotropic tissue structure on reentrant circuits in the epicardial border zone of subacute canine infarcts. Circ Res. 1988;63:182-206.

56. Efimov IR, Aguel F, Cheng Y, Wollenzier B, Trayanova N: Virtual electrode polarization in the far field: implications for external defibrillation. Am J Physiol Heart Circ Physiol. 2000;279:H1055-1070.

57. Trayanova NA: Effects of the tissue-bath interface on the induced transmembrane potential: a modeling study in cardiac stimulation. Ann Biomed Eng. 1997;25:783-792.

58. Cheng Y, Mowrey KA, Van Wagoner DR, Tchou PJ, Efimov IR: Virtual electrode-induced reexcitation: A mechanism of defibrillation. Circ Res. 1999;85:1056-1066.

59. Ho SY, Jackson M, Kilpatrick L, Smith A, Gerlis LM: Fibrous matrix of ventricular myocardium in tricuspid atresia compared with normal heart. A quantitative analysis. Circulation. 1996;94:1642-1646.